Continuous and discontinuous finite element methods for coupled surface-subsurface flow and transport problems

Aycil Cesmelioglu, Prince Chidyagwai and Béatrice Rivière *

Abstract

A weak formulation of the coupled problem of flow and transport is discretized and analyzed numerically. The flow problem is characterized by the Navier-Stokes (or Stokes) equations coupled by Darcy equations. The velocity field is obtained by couplings of finite element and discontinuous Galerkin methods. The concentration equation is solved by an improved discontinuous Galerkin method. Convergence of the schemes is obtained. Numerical examples show the robustness of the method for heterogeneous and fractured porous media.

1 Introduction

The study of a coupled flow and transport system in adjacent surface and subsurface regions is of interest for the environmental problem of contaminated aquifers through rivers. The flow in the surface region is characterized by the steady-state Navier-Stokes (or Stokes) equations whereas the flow in the subsurface region is characterized by the Darcy's law. The transport equation is coupled to the flow problem in the sense that the flow velocity appears in both the diffusion and the convection terms of the concentration equation. This type of multiphysics couplings is also of importance in the industrial filtration processes [20].

This paper follows a series of papers on the coupled surface/subsurface flow by the authors. In [18, 11, 10, 9, 8], the flow problem coupling Navier-Stokes equations with Darcy equations was analyzed numerically and theoretically for different interface conditions, and different numerical discretizations. The usual interface conditions include the Beavers-Joseph-Saffman law [5, 27], the continuity of normal component of velocity, and the balance of forces across the interface. In [7], well-posedness of a weak formulation of the coupled flow and transport equation is obtained. The main objective of this paper is to propose robust numerical schemes for approximation of the weak solution. We assume the coupling to be a one-way coupling, in the sense that the velocity field obtained from solving the surface/subsurface flow problem becomes an input data for the transport problem.

The flow problem is approximated by either the Discontinuous Galerkin (DG) method, the continuous Finite Element Method (FEM) or a combination of the two. Because of its flexibility and local mass conservation property, the DG method is a well-suited method for the coupled surface/subsurface problem. The DG solution is compared to the FEM solution, which is less computationally costly. A multinumerics approach is also considered, in which the Navier-Stokes equations are discretized by the FEM, and the Darcy equations by the DG method. This third approach has the advantage to combine FEM legacy codes for solving the Navier-Stokes equations with a DG code, known to be robust for simulating single phase flow in heterogeneous media.

The transport problem is solved by a discontinuous Galerkin method that upwinds the numerical fluxes in the subsurface region [25]. In this case, one does not need to use slope limiters.

The coupled surface/subsurface flow problem has recently gained a lot of interest in the scientific community. Most of the published literature deals with the coupling of Stokes and Darcy equations (see for instance

*Rice University, Department of Computational and Applied Mathematics, 6100 Main St MS-134, Houston, TX 77005, U.S.A.
The authors acknowledge the support of National Science Foundation through the grant DMS 0810422.

[22, 15, 14, 16, 24]. The published literature is very sparse on the coupling of Stokes-Darcy-transport problem. In [28], a mixed method is proposed for the coupled Stokes/Darcy equations and a local discontinuous Galerkin method [13] is used for the transport problem.

The outline of the paper is as follows. The next section introduces the model problem and its weak formulation. In Section 3, the numerical schemes are defined and error estimates are obtained. Numerical examples are shown in Section 4. Conclusions follow.

2 Model problem

For simplicity we assume that the surface region is contained in a domain $\Omega_1 \subset \mathbb{R}^2$ and the subsurface region in a domain $\Omega_2 \subset \mathbb{R}^2$. Let $\boldsymbol{u}_i$ and p_i denote the fluid velocity and pressure in Ω_i, for $i = 1, 2$. Let $\boldsymbol{\tau}_{12}$ and $\boldsymbol{n}_{12}$ be a unit tangential vector and a unit normal vector at the interface $\Gamma_{12} = \partial\Omega_1 \cap \partial\Omega_2$. The vector $\boldsymbol{n}_{12}$ is assumed to be outward of Ω_1. The surface/subsurface flow is characterized by the following Navier-Stokes equations coupled with the Darcy equations, and appropriate interface conditions.

$$-\nabla \cdot (2\mu \boldsymbol{D}(\boldsymbol{u}_1)) + \nabla p_1 + \boldsymbol{u}_1 \cdot \nabla \boldsymbol{u}_1 = \boldsymbol{f}_1, \qquad \nabla \cdot \boldsymbol{u}_1 = 0, \text{ in } \Omega_1, \tag{1}$$

$$\boldsymbol{u}_2 = -\frac{\boldsymbol{K}}{\mu}(\nabla p_2 - \rho \boldsymbol{g}), \qquad \nabla \cdot \boldsymbol{u}_2 = f_2, \text{ in } \Omega_2, \tag{2}$$

$$\boldsymbol{u}_1 \cdot \boldsymbol{n}_{12} = \boldsymbol{u}_2 \cdot \boldsymbol{n}_{12}, \text{ on } \Gamma_{12}, \tag{3}$$

$$G\boldsymbol{K}^{-1/2}\boldsymbol{u}_1 \cdot \boldsymbol{\tau}_{12} = -2\mu \boldsymbol{D}(\boldsymbol{u}_1)\boldsymbol{n}_{12} \cdot \boldsymbol{\tau}_{12}, \text{ on } \Gamma_{12}, \tag{4}$$

$$(-2\mu \boldsymbol{D}(\boldsymbol{u}_1)\boldsymbol{n}_{12}) \cdot \boldsymbol{n}_{12} + p_1 = p_2, \text{ on } \Gamma_{12}. \tag{5}$$

Let $\boldsymbol{u}$ denote the velocity field over the whole domain, namely $\boldsymbol{u}|_{\Omega_i} = \boldsymbol{u}_i$. The concentration c of one species transported in the domain $\Omega = \Omega_1 \cup \Omega_2$ over the time interval $(0, T)$ satisfies the following equation

$$\frac{\partial}{\partial t}(\varphi c) - \nabla \cdot (\boldsymbol{F}(\boldsymbol{u})\nabla c - c\boldsymbol{u}) = f, \quad \text{in } (0, T) \times \Omega. \tag{6}$$

We remark that if the nonlinear term $\boldsymbol{u}_1 \cdot \nabla \boldsymbol{u}_1$ is removed from the momemtum equation in (1), the resulting problem is a coupled Stokes-Darcy flow with transport, and (1) is replaced by:

$$-\nabla \cdot (2\mu \boldsymbol{D}(\boldsymbol{u}_1)) + \nabla p_1 = \boldsymbol{f}_1, \qquad \nabla \cdot \boldsymbol{u}_1 = 0, \quad \text{in } \Omega_1.$$

Throughout the paper, we will point out the simplifications obtained if the Stokes equations are used instead of the Navier-Stokes equations in the free flow region. Define $\Gamma_i = \partial\Omega_i \setminus \Gamma_{12}$ and denote by $\boldsymbol{n}$ the unit outward normal to $\partial\Omega$. The system of equations is completed by boundary conditions and an initial condition for the concentration.

$$\boldsymbol{u}_1 = \boldsymbol{0}, \text{ on } \Gamma_1, \tag{7}$$

$$\boldsymbol{u}_2 \cdot \boldsymbol{n} = \mathcal{U}, \text{ on } \Gamma_2, \tag{8}$$

$$\boldsymbol{F}(\boldsymbol{u})\nabla c \cdot \boldsymbol{n} - c\boldsymbol{u} \cdot \boldsymbol{n} = -\mathcal{C}\boldsymbol{u} \cdot \boldsymbol{n}, \text{ on } (0, T) \times \{x \in \partial\Omega : \mathcal{U}(x) < 0\}, \tag{9}$$

$$\boldsymbol{F}(\boldsymbol{u})\nabla c \cdot \boldsymbol{n} = 0, \text{ on } (0, T) \times \{x \in \partial\Omega : \mathcal{U}(x) \geq 0\}, \tag{10}$$

$$c = c_0, \text{ in } \{0\} \times \Omega. \tag{11}$$

We now describe the coefficients that appear in the equations above.

- The fluid kinematic viscosity μ and fluid density ρ are positive constants. The vector of gravitational acceleration is denoted by $\boldsymbol{g}$.
- The rate of strain matrix is symmetric and defined by $\boldsymbol{D}(\boldsymbol{u}) = 0.5(\nabla \boldsymbol{u} + (\nabla \boldsymbol{u})^T)$.
- The vector function $\boldsymbol{f}_1$ and scalar functions f_2 and f represent the source/sink terms.

- The permeability $\boldsymbol{K}$ is a symmetric positive definite matrix bounded above and below: there exist $\underline{k} > 0, \bar{k} > 0$ such that
$$\forall \xi \in \mathbb{R}^2, \quad \underline{k}\xi \cdot \xi \leq \xi \cdot \boldsymbol{K}\xi \leq \bar{k}\xi \cdot \xi.$$

- The coefficient G that appears in the interface condition (4) is a positive constant. It is obtained experimentally and depends on the properties of the fluid and the porous medium.

- The coefficient φ is a positive constant bounded by one. Restricted to Ω_2, the value of φ corresponds to the porosity of the subsurface. By convention, the coefficient φ is simply equal to one on Ω_1.

- The coefficient $\boldsymbol{F}(\boldsymbol{u})$ is a diffusion/dispersion matrix. In Ω_1, it is simply equal to $d_m\boldsymbol{I}$, where d_m is a positive constant, and $\boldsymbol{I}$ is the identity matrix. In the porous region Ω_2, the matrix $\boldsymbol{F}(\boldsymbol{u})$ depends on the velocity in the following manner:
$$\boldsymbol{F}(\boldsymbol{u}) = (\alpha_T\|\boldsymbol{u}\| + d_m)\boldsymbol{I} + (\alpha_l - \alpha_t)\frac{\boldsymbol{u}\boldsymbol{u}^T}{\|\boldsymbol{u}\|}.$$
The coefficient $d_m > 0$ is the molecular diffusivity constant, $\alpha_l \geq 0$ and $\alpha_t \geq 0$ are the longitudinal and transverse dispersivities and $\|\cdot\|$ denotes the Euclidean norm. One can show that there exist $\alpha > 0, M > 0$ such that
$$\boldsymbol{F}(\boldsymbol{w})\psi \cdot \psi \geq \alpha\psi \cdot \psi, \quad \|\boldsymbol{F}(\boldsymbol{w})\| \leq M\|\boldsymbol{w}\|. \tag{12}$$
In addition, we assume that there is $\bar{F} > 0$ such that
$$\|\boldsymbol{F}(\boldsymbol{w})\| \leq \bar{F}. \tag{13}$$

- The boundary flux $\mathcal{U}$ belongs to $L^2(\Gamma_2)$. The data f_2 and $\mathcal{U}$ must satisfy the compatibility condition
$$\int_{\Gamma_2} \mathcal{U} = \int_{\Omega_2} f_2.$$

- The function $\mathcal{C} \geq 0$ is the prescribed concentration on the inflow boundary. It is assumed to be bounded. For any function z, we denote $z^+ = \max(0, z)$ and $z^- = \max(0, -z)$. Extending $\mathcal{U}$ to zero on Γ_1, we can rewrite the boundary conditions (9), (10) as
$$\boldsymbol{F}(\boldsymbol{u})\nabla c \cdot \boldsymbol{n} + c(\boldsymbol{u} \cdot \boldsymbol{n})^- = \mathcal{C}\mathcal{U}^- \text{ on } (0, T) \times \partial\Omega. \tag{14}$$

- The initial concentration c_0 is nonnegative and bounded.

We will solve for the unknowns $(\boldsymbol{u}_1, p_1, p_2, c)$. We note that the Darcy velocity $\boldsymbol{u}_2$ can be obtained from the Darcy pressure p_2 via the first equation in (2). For any domain $\mathcal{O}$, the standard notation for the $L^k(\mathcal{O})$ spaces and Sobolev spaces $H^k(\mathcal{O})$ is used. The L^2 inner-product of two functions is denoted by $(\cdot, \cdot)_{\mathcal{O}}$. Let $H^1_{0,\Gamma_1}(\Omega_1)$ denote the space of functions in $H^1(\Omega_1)$ whose trace vanishes on Γ_1. The dual space of $H^1(\Omega)$ is denoted by $H^1(\Omega)'$ and the duality pairing is $\langle \cdot, \cdot \rangle_{(H^1(\Omega)', H^1(\Omega))}$.

A weak solution to the problem (1)-(8) with (11) and (14) is the quadruple $(\boldsymbol{u}_1, p_1, p_2, c) \in H^1_{0,\Gamma_1}(\Omega_1)^2 \times L^2(\Omega_1) \times H^1(\Omega_2) \times (L^2(0, T; H^1(\Omega)) \cap L^\infty((0, T) \times \Omega))$ satisfying:

$$\forall \boldsymbol{v}_1 \in H^1_{0,\Gamma_1}(\Omega_1)^2, \forall q_1 \in L^2(\Omega_1), \forall q_2 \in H^1(\Omega_2), \quad 2\mu(\boldsymbol{D}(\boldsymbol{u}_1), \boldsymbol{D}(\boldsymbol{v}_1))_{\Omega_1} + (\boldsymbol{u}_1 \cdot \nabla\boldsymbol{u}_1, \boldsymbol{v}_1)_{\Omega_1} + (\frac{\boldsymbol{K}}{\mu}\nabla p_2, \nabla q_2)_{\Omega_2}$$
$$-(\nabla \cdot \boldsymbol{v}_1, p_1)_{\Omega_1} + (p_2, \boldsymbol{v}_1 \cdot \boldsymbol{n}_{12})_{\Gamma_{12}} + G(\boldsymbol{K}^{-1/2}\boldsymbol{u}_1 \cdot \boldsymbol{\tau}_{12}, \boldsymbol{v}_1 \cdot \boldsymbol{\tau}_{12})_{\Gamma_{12}}$$
$$-(\boldsymbol{u}_1 \cdot \boldsymbol{n}_{12}, q_2)_{\Gamma_{12}} + (\nabla \cdot \boldsymbol{u}_1, q_1)_{\Omega_1} = (\boldsymbol{f}_1, \boldsymbol{v}_1)_{\Omega_1} + (f_2 + \frac{\boldsymbol{K}}{\mu}\rho\boldsymbol{g}, q_2)_{\Omega_2} - (\mathcal{U}, q_2)_{\Gamma_2}, \tag{15}$$

$$\forall z \in L^2(0,T;H^1(\Omega)), \quad \int_0^T \langle \varphi \frac{\partial c}{\partial t}, z\rangle_{(H^1(\Omega)', H^1(\Omega))} dt - \int_0^T (c\boldsymbol{u}, \nabla z)_\Omega dt$$

$$+ \int_0^T (\boldsymbol{F}(\boldsymbol{u})\nabla c, \nabla z)_\Omega dt + \int_0^T ((c\mathcal{U}^+ - \mathcal{C}\mathcal{U}^-), z)_{\partial\Omega} dt = \int_0^T (f,z)_\Omega dt. \tag{16}$$

$$t \to c(t,\cdot) \in \mathcal{C}^0([0,T];(H^1(\Omega))'), \quad t \to \frac{\partial c}{\partial t}(t,\cdot) \in L^2(0,T;(H^1(\Omega))'), \quad c(0,\cdot) = c_0(\cdot) \text{ a.e. in } \Omega. \tag{17}$$

Because only Neumann boundary conditions hold for the flow problem, the additional constraint $\int_{\Omega_2} p_2 = 0$ is imposed. Existence of a weak solution can be derived by combining results from [2, 18, 23]. We state the result below.

Theorem 2.1. *Assume that $\boldsymbol{f}_1 \in L^2(\Omega_1)^2$, $f_2 \geq 0$, $f_2 \in L^2(\Omega_2)$ and $f \geq 0$, $f \in L^1(0,T;L^\infty(\Omega)) \cap L^2(0,T;L^2(\Omega))$. There exists a constant $\tilde{M} > 0$ such that if*

$$\mu^2 > \tilde{M}(\|\boldsymbol{f}_1\|^2_{L^2(\Omega_1)} + \mu\|f_2\|^2_{L^2(\Omega_2)} + \mu\|\mathcal{U}\|^2_{L^2(\Gamma_2)} + \|\boldsymbol{g}\|^2_{L^2(\Omega_2)}) \tag{18}$$

then there exists a weak solution $(\boldsymbol{u}_1, p_1, p_2, c)$ to the weak problem (15)-(17).

Remark: If the Stokes equations are used, existence of the weak solution is unconditional, i.e. there is no need to assume small data condition like (18). This result is a consequence of the more general coupling analyzed in [7]. The same result holds true if the Navier-Stokes equations are used and the interface condition (5) is replaced by

$$(-2\mu\boldsymbol{D}(\boldsymbol{u}_1)\boldsymbol{n}_{12}) \cdot \boldsymbol{n}_{12} + p_1 + \frac{1}{2}\boldsymbol{u}_1 \cdot \boldsymbol{u}_1 = p_2.$$

In this case, the coupled flow model is numerically discussed in [10].

In the next section, we define several numerical approximations of the weak problem.

3 Numerical Discretization

Let $\mathcal{E}^h$ be a regular family of triangulations of $\overline{\Omega}$ (see [12]) and let h denote the maximum diameter of the triangles. We assume that the interface Γ_{12} is a finite union of triangle edges. Therefore, the restriction of $\mathcal{E}^h$ to Ω_i is also a regular family of triangulations of $\overline{\Omega}_i$; we denote it by $\mathcal{E}_i^h$ and impose that the two meshes $\mathcal{E}_i^h$ coincide at the interface Γ_{12}. This restriction simplifies the analysis, but it can be relaxed.

For $i = 1, 2$, let Γ_i^h denote the set of edges of $\mathcal{E}_i^h$ interior to Ω_i and let $\Gamma^h = \Gamma_1^h \cup \Gamma_2^h$. To each edge e of $\mathcal{E}^h$ we associate once and for all a unit normal vector $\boldsymbol{n}_e$. For the edges in Γ_i^h, this can be done by ordering the triangles of $\mathcal{E}_i^h$ and orienting the normal in the direction of increasing numbers. For $e \in \Gamma_{12}$, we set $\boldsymbol{n}_e = \boldsymbol{n}_{12}$, i.e. $\boldsymbol{n}_e$ is the exterior normal to Ω_1. For a boundary edge $e \in \Gamma_i$, $\boldsymbol{n}_e$ coincides with the outward normal vector $\boldsymbol{n}$ to $\partial\Omega$. If $\boldsymbol{n}_e$ points from the element E^1 to the element E^2, the jump $[\cdot]$ and average $\{\cdot\}$ of a function ϕ are given by:

$$[\phi] = \phi|_{E^1} - \phi|_{E^2}, \quad \{\phi\} = \frac{1}{2}\phi|_{E^1} + \frac{1}{2}\phi|_{E^2}.$$

By convention, for a boundary edge on Γ_i, the jump and average are defined to be equal to the trace of the function on that edge. The length of an edge e is denoted by $|e|$.

3.1 Numerical Approximation of Flow Problem

Let $\boldsymbol{X}_1^h, Q_1^h, Q_2^h$ be finite dimensional subspaces to be defined later. Formally, the discrete weak formulation of (1)-(5) can be written as: find $\boldsymbol{U}_1^h \in \boldsymbol{X}_1^h, P_1^h \in Q_1^h, P_2^h \in Q_2^h$ such that

$$\begin{aligned}
\forall \boldsymbol{v}_1^h \in \boldsymbol{X}_1^h, \forall q_2^h \in Q_2^h, \quad & a_{\mathrm{NS}}(\boldsymbol{U}_1^h, \boldsymbol{v}_1^h) + b_{\mathrm{NS}}(\boldsymbol{v}_1^h, P_1^h) + c_{\mathrm{NS}}(\boldsymbol{U}_1^h; \boldsymbol{U}_1^h, \boldsymbol{v}_1^h) + a_{\mathrm{D}}(P_2^h, q_2^h) \\
& + \gamma(\boldsymbol{U}_1^h, P_2^h; \boldsymbol{v}_1^h, q_2^h) = \ell(\boldsymbol{v}_1^h, q_2^h), \\
\forall q_1^h \in Q_1^h, \quad & b_{\mathrm{NS}}(\boldsymbol{U}_1^h, q_1^h) = 0, \\
& \int_{\Omega_2} P_2^h = 0,
\end{aligned}$$

where $a_{\mathrm{NS}}, b_{\mathrm{NS}}, c_{\mathrm{NS}}, a_{\mathrm{D}}$ are discretizations of the operators $-\nabla\cdot(2\mu\boldsymbol{D}(\boldsymbol{u}))$, ∇p, $\boldsymbol{u}\cdot\nabla\boldsymbol{u}$ and $-\nabla\cdot((\boldsymbol{K}/\mu)\nabla p)$ respectively. These forms depend on the choice of the method and we will give several examples in the following sections. Since the discrete problem is steady-state and nonlinear, Picard iterations are computed with an initial zero Navier-Stokes velocity.

Denote by $\boldsymbol{U}^h$ the resulting velocity field of the coupled Navier-Stokes and Darcy equations. The velocity $\boldsymbol{U}^h$ is defined in Ω by:

$$\boldsymbol{U}^h = \begin{cases} \boldsymbol{U}_1^h, & \text{in } \Omega_1 \\ -\frac{\boldsymbol{K}}{\mu}(\nabla P_2^h - \rho\boldsymbol{g}), & \text{in } \Omega_2 \end{cases} \tag{19}$$

The form γ couples the two different physical flows through the interface Γ_{12}.

$$\gamma(\boldsymbol{U}_1^h, P_2^h; \boldsymbol{v}_1^h, q_2^h) = (P_2^h, \boldsymbol{v}_1^h\cdot\boldsymbol{n}_{12})_{\Gamma_{12}} + G(\boldsymbol{K}^{-1/2}\boldsymbol{U}_1^h\cdot\boldsymbol{\tau}_{12}, \boldsymbol{v}_1^h\cdot\boldsymbol{\tau}_{12})_{\Gamma_{12}} - (\boldsymbol{U}_1^h\cdot\boldsymbol{n}_{12}, q_2^h)_{\Gamma_{12}}. \tag{20}$$

The form ℓ is defined as:

$$\ell(\boldsymbol{v}_1^h, q_2^h) = (\boldsymbol{f}_1, \boldsymbol{v}_1^h)_{\Omega_1} + (f_2 + \frac{\boldsymbol{K}}{\mu}\rho\boldsymbol{g}, q_2^h)_{\Omega_2} + (\mathcal{U}, q_2^h)_{\Gamma_2}.$$

We remark that if the Stokes equations are used instead of the Navier-Stokes equations, the numerical scheme remains the same with the choice $c_{\mathrm{NS}} = 0$. One can use various discretizations in either subdomains. We choose to present the discontinuous Galerkin (DG) method, the finite element method (FEM) and a combination of the two. In what follows we give a description of the linear forms $a_{\mathrm{NS}}, a_{\mathrm{D}}, b_{\mathrm{NS}}, c_{\mathrm{NS}}$.

3.1.1 DG scheme

The primal DG method is applied to both the Navier-Stokes equations and the Darcy equations. The penalty parameter is denoted by $\sigma > 0$ and the symmetrizing parameter by ϵ. The parameter ϵ takes the values -1 or $+1$, which corresponds to either the symmetric interior penalty Galerkin (SIPG) method or the non-symmetric interior penalty Galerkin (NIPG) method [29, 3, 26]. We can allow for different values of σ for each edge, and for different values of ϵ for the forms a_{NS} and a_{D}. To simplify the text, we assume that σ and ϵ are fixed constants for both forms. Let k_1, k_2 be positive integers, each greater than or equal to one. In that case the finite dimensional spaces are

$$\boldsymbol{X}_1^h = \{\boldsymbol{v}_h \in L^2(\Omega_1)^2 : \boldsymbol{v}_h|_E \in (\mathbb{P}_{k_1}(E))^2, \forall E\in\mathcal{E}_1^h\}, \quad Q_1^h = \{q_h \in L^2(\Omega_1) : q_h|_E \in \mathbb{P}_{k_1-1}(E), \forall E\in\mathcal{E}_1^h\},$$
$$Q_2^h = \{q_h \in L^2(\Omega_2) : q_h|_E \in \mathbb{P}_{k_2}(E), \forall E\in\mathcal{E}_2^h\},$$

where $\mathbb{P}_k$ is the space of polynomials of degree less than or equal to k and the forms are:

$$\begin{aligned} a_{\mathrm{NS}}(\boldsymbol{w}_h, \boldsymbol{v}_h) &= 2\mu\sum_{E\in\mathcal{E}_1^h}(\boldsymbol{D}(\boldsymbol{w}_h), \boldsymbol{D}(\boldsymbol{v}_h))_E - 2\mu\sum_{e\in\Gamma_1^h\cup\Gamma_1}(\{\boldsymbol{D}(\boldsymbol{w}_h)\boldsymbol{n}_e\}, [\boldsymbol{v}_h])_e \\ &+2\epsilon\mu\sum_{e\in\Gamma_1^h\cup\Gamma_1}(\{\boldsymbol{D}(\boldsymbol{v}_h)\boldsymbol{n}_e\}, [\boldsymbol{w}_h])_e + \mu\sum_{e\in\Gamma_1^h\cup\Gamma_1}\frac{\sigma}{|e|}([\boldsymbol{w}], [\boldsymbol{v}])_e, \end{aligned} \tag{21}$$

$$b_{\mathrm{NS}}(\boldsymbol{v}_h, q_1^h) = -\sum_{E\in\mathcal{E}_1^h}(q_1^h, \nabla\cdot\boldsymbol{v}_h)_E + \sum_{e\in\Gamma_1^h\cup\Gamma_1}(\{q_1^h\}, [\boldsymbol{v}_h]\cdot\boldsymbol{n}_e)_e, \tag{22}$$

$$\begin{aligned} a_{\mathrm{D}}(z_2^h, q_2^h) &= \sum_{E\in\mathcal{E}_2^h}(\frac{\boldsymbol{K}}{\mu}\nabla z_2^h, \nabla q_2^h)_E - \sum_{e\in\Gamma_2^h}(\{\frac{\boldsymbol{K}}{\mu}\nabla z_2^h\cdot\boldsymbol{n}_e\}, [q_2^h])_e \\ &+\epsilon\sum_{e\in\Gamma_2^h}(\{\frac{\boldsymbol{K}}{\mu}\nabla q_2^h\cdot\boldsymbol{n}_e\}, [z_2^h])_e + \sum_{e\in\Gamma_2^h}\frac{\sigma}{|e|}([z_2^h], [q_2^h])_e. \end{aligned} \tag{23}$$

The DG discretization of the nonlinear term $\boldsymbol{u}\cdot\boldsymbol{u}$ has been studied extensively, for instance in [19]. For this, we introduce additional notation. For an element $E\in\mathcal{E}^h$, let $\mathcal{N}(E)$ denote the neighboring element sharing part of ∂E. When the side of E belongs to $\partial\Omega$, then $\mathcal{N}(E)$ is not defined, and by convention we set $\boldsymbol{v}_h|_{\mathcal{N}(E)} = \boldsymbol{0}$ for any function $\boldsymbol{v}_h \in \boldsymbol{X}_1^h$. We also denote by $\boldsymbol{n}_E$ the unit outward normal to E. The inflow boundary of E with respect to a function $\boldsymbol{z}_h \in \boldsymbol{X}_1^h$ is defined by

$$\partial E_-(\boldsymbol{z}_h) = \{\boldsymbol{x} \in \partial E \,:\, \{\boldsymbol{z}_h(\boldsymbol{x})\} \cdot \boldsymbol{n}_E < 0\}.$$

We are now ready to define the form c_{NS}.

$$\begin{aligned} c_{\mathrm{NS}}(\boldsymbol{z}_h; \boldsymbol{v}_h, \boldsymbol{w}_h) &= \sum_{E\in\mathcal{E}_1^h} (\boldsymbol{z}_h \cdot \nabla \boldsymbol{v}_h, \boldsymbol{w}_h)_E + \frac{1}{2} \sum_{E\in\mathcal{E}_1^h} (\nabla \cdot \boldsymbol{z}_h, \boldsymbol{v}_h \cdot \boldsymbol{w}_h)_E \\ -\frac{1}{2} \sum_{e\in\Gamma_1^h\cup\Gamma_1} ([\boldsymbol{z}_h] \cdot \boldsymbol{n}_e, \{\boldsymbol{v}_h \cdot \boldsymbol{w}_h\})_e &+ \sum_{E\in\mathcal{E}_1^h} (\{\boldsymbol{z}_h\} \cdot \boldsymbol{n}_E (\boldsymbol{v}_h|_E - \boldsymbol{v}_h|_{\mathcal{N}(E)}), \boldsymbol{w}_h|_E)_{\partial E_-(\boldsymbol{z}_h)\setminus\Gamma_{12}}. \end{aligned} \tag{24}$$

The norms associated with the discrete spaces are:

$$\|\boldsymbol{v}\|_{\boldsymbol{X}_1^h} = \left(\sum_{E\in\mathcal{E}_1^h} \|D(\boldsymbol{v})\|^2_{L^2(E)} + \sum_{e\in\Gamma_1^h\cup\Gamma_1} |e|^{-1} \|[\boldsymbol{v}]\|^2_{L^2(e)} \right)^{1/2},$$

$$\|q\|_{Q_1^h} = \|q\|_{L^2(\Omega_1)},$$

$$\|q\|_{Q_2^h} = \left(\sum_{E\in\mathcal{E}_2^h} \|\frac{\boldsymbol{K}^{1/2}}{\mu^{1/2}} \nabla q\|^2_{L^2(E)} + \sum_{e\in\Gamma_2^h} |e|^{-1} \|[q]\|^2_{L^2(e)} \right)^{1/2}.$$

3.1.2 FEM scheme

In this second approach, the discrete spaces $\boldsymbol{X}_1^h \subset (H_0^1(\Omega_1))^2, Q_1^h \subset L_0^2(\Omega_1)$, and $Q_2^h \subset H^1(\Omega_2)$ are conforming spaces of order k_1 for Ω_1 and k_2 for Ω_2. For instance, to approximate the Navier-Stokes velocity and pressure, one can use the MINI elements [4] of order one or the Taylor-Hood elements [21] of order two. These spaces satisfy an inf-sup condition, with an inf-sup constant independent of h. In these two cases, the Darcy pressure space consists of continuous piecewise linears

$$Q_2^h = \{q_h \in \mathcal{C}(\overline{\Omega}_2) : \, q_h|_E \in \mathbb{P}_1(E), \forall E \in \mathcal{E}_2^h\}.$$

The bilinear forms are

$$a_{\mathrm{NS}}(\boldsymbol{v}_h, \boldsymbol{w}_h) = 2\mu(\boldsymbol{D}(\boldsymbol{v}_h), \boldsymbol{D}(\boldsymbol{w}_h))_{\Omega_1}, \tag{25}$$

$$b_{\mathrm{NS}}(\boldsymbol{v}_h, q_1^h) = -(q_1^h, \nabla \cdot \boldsymbol{v}_h)_{\Omega_1}, \tag{26}$$

$$a_{\mathrm{D}}(z_2^h, q_2^h) = (\boldsymbol{K}\nabla z_2^h, \nabla q_2^h)_{\Omega_2}, \tag{27}$$

$$c_{\mathrm{NS}}(\boldsymbol{z}_h; \boldsymbol{v}_h, \boldsymbol{w}_h) = \frac{1}{2}(\boldsymbol{z}_h \cdot \nabla \boldsymbol{v}_h, \boldsymbol{w}_h)_{\Omega_1} - \frac{1}{2}(\boldsymbol{z}_h \cdot \nabla \boldsymbol{w}_h, \boldsymbol{v}_h)_{\Omega_1} + \frac{1}{2}(\boldsymbol{z}_h \cdot \boldsymbol{n}_{12}, \boldsymbol{v}_h \cdot \boldsymbol{w}_h)_{\Gamma_{12}}. \tag{28}$$

The FEM spaces are equipped with the following norms:

$$\|\boldsymbol{v}\|_{\boldsymbol{X}_1^h} = \|\boldsymbol{D}(\boldsymbol{v})\|_{L^2(\Omega_1)}, \quad \|q\|_{Q_1^h} = \|q\|_{L^2(\Omega_1)}, \quad \|q\|_{Q_2^h} = \|\frac{\boldsymbol{K}^{1/2}}{\mu^{1/2}} \nabla q\|_{L^2(\Omega_2)}.$$

3.1.3 FEM/DG scheme

In this third approach, we propose to employ the FEM to solve the Navier-Stokes equations in Ω_1 and to employ the DG method to solve the Darcy equations in Ω_2. Conforming element spaces of order k_1 are used for the spaces $\boldsymbol{X}_1^h$ and Q_1^h, and discontinuous piecewise polynomials of degree k_2 are used for the space Q_2^h. The bilinear forms are the forms defined by (25), (26), (28) and (23).

3.1.4 Error analysis

The DG method and the FEM/DG method were analyzed in [18, 10] for different boundary conditions for the Darcy pressure. It is a technicality to redo the analysis for the case of Neumann boundary condition. A similar analysis can be done for the FEM method. Existence and uniqueness of the numerical solution $(\boldsymbol{U}_1^h, P_1^h, P_2^h)$ are obtained under small data condition similar to (18). Convergence rates are optimal. More precisely, there is a constant M independent of h such that

$$\|\boldsymbol{u}_1 - \boldsymbol{U}_1^h\|_{\boldsymbol{X}_1^h} + \|p_1 - P_1^h\|_{Q_1^h} + \|p_2 - P_2^h\|_{Q_2^h} \leq M(h^{k_1} + h^{k_2}). \tag{29}$$

Using (19) and the fact that $\|\cdot\|_{L^2(\Omega_1)} \leq M\|\cdot\|_{\boldsymbol{X}_1^h}$ (see [19]), we obtain an error bound of the velocity field in the L^2-norm.

$$\|\boldsymbol{u} - \boldsymbol{U}^h\|_{L^2(\Omega)} \leq M(h^{k_1} + h^{k_2}). \tag{30}$$

As a consequence, using a trace theorem, an inverse inequality, and the Lagrange interpolant of $\boldsymbol{u}$, we have

$$\forall e \in \Gamma^h, \quad \|\boldsymbol{u} - \boldsymbol{U}^h\|_{L^2(e)} \leq M(h^{k_1-1/2} + h^{k_2-1/2}). \tag{31}$$

One can also show that the velocity $\boldsymbol{U}^h$ is bounded in the L^2 norm by the data: there is a constant $\overline{M} > 0$ independent of h, but dependent on the data μ, $\|\boldsymbol{f}_1\|_{L^2(\Omega_1)}$, $\|f_2\|_{L^2(\Omega_2)}$ and $\|\mathcal{U}\|_{L^2(\partial\Omega)}$, such that

$$\|\boldsymbol{U}^h\|_{L^2(\Omega)} \leq \overline{M}. \tag{32}$$

Remark: If the Stokes equations are used instead of the Navier-Stokes equations, existence and uniqueness of the numerical solution is unconditional.

3.2 Numerical Approximation of Transport Problem

The equation (6) is discretized by a combined backward Euler and DG method. Let Δt be a positive time step and let $t^j = j\Delta t$ denote the time at the j^{th} step. Let Q_h denote the space of discontinuous piecewise polynomials of degree r. The approximation of the initial concentration is obtained by an L^2 projection:

$$\forall q_h \in Q_h, \quad (C_0^h, q_h)_\Omega = (c_0, q_h)_\Omega.$$

For any $j \geq 0$, the approximation C_{j+1}^h of the concentration c at time t^{j+1} is defined by the following discrete variational problem.

$$\forall q_h \in Q_h, \quad \varphi(\frac{C_{j+1}^h - C_j^h}{\Delta t}, q_h)_\Omega + a_T(\boldsymbol{U}^h; C_{j+1}^h, q_h) + d_T(\boldsymbol{U}^h; C_{j+1}^h, q_h) = L_T(t^{j+1}; q_h), \tag{33}$$

where the bilinear form a_T is a DG discretization of the operator $-\nabla\cdot(\boldsymbol{F}(\boldsymbol{u})\nabla c)$ and the bilinear form d_T is a DG discretization of the operator $\nabla\cdot(\boldsymbol{u}c)$. Before defining these forms, we introduce the upwind value $q_h^\uparrow$ of a function q_h in Q_h with respect to the velocity field $\boldsymbol{U}^h$, defined by (19). Let e be an edge shared by the elements E_1 and E_2 and assume the unit normal vector $\boldsymbol{n}_e$ points outward of E_1.

$$q_h^\uparrow = \begin{cases} q_h|_{E_1} & \text{if } \{\boldsymbol{U}^h\}\cdot\boldsymbol{n}_e > 0, \\ q_h|_{E_2} & \text{if } \{\boldsymbol{U}^h\}\cdot\boldsymbol{n}_e \leq 0. \end{cases}$$

The penalty parameter is denoted by σ. The symmetrization parameter is denoted by $\epsilon \in \{-1, 1\}$. The forms a_T, d_T, L_T are given below for any θ_h, q_h in Q_h:

$$\begin{aligned}
a_T(\boldsymbol{U}^h; \theta_h, q_h) &= \sum_{E\in\mathcal{E}^h} (\boldsymbol{F}(\boldsymbol{U}^h)\nabla\theta_h, \nabla q_h)_E + \sum_{e\in\Gamma^h} |e|^{-1}(\sigma[\theta_h], [q_h])_e - \sum_{e\in\Gamma^h} ((\boldsymbol{F}(\boldsymbol{U}^h)\nabla\theta_h\cdot\boldsymbol{n}_e)^\uparrow, [q_h])_e \\
&+ \epsilon \sum_{e\in\Gamma^h} ((\boldsymbol{F}(\boldsymbol{U}^h)\nabla q_h\cdot\boldsymbol{n}_e)^\uparrow, [\theta_h])_e + \sum_{e\in\partial\Omega} (\theta_h, \mathcal{U}^+ q_h)_e, \\
d_T(\boldsymbol{U}^h; \theta_h, q_h) &= -\sum_{E\in\mathcal{E}^h} (\theta_h \boldsymbol{U}^h, \nabla q_h)_E + \sum_{e\in\Gamma^h} (\theta_h^\uparrow\{\boldsymbol{U}^h\cdot\boldsymbol{n}_e\}, [q_h])_e, \\
L_T(t^{j+1}; q_h) &= \int_\Omega f(t^{j+1}) q_h + \int_{\partial\Omega} \mathcal{C}(t^{j+1})\mathcal{U}^- q_h.
\end{aligned}$$

This scheme uses an improved DG method in which the diffusive fluxes are upwinded whereas in the standard DG method the diffusive fluxes are averaged. The improved method is more stable and does not require the use of slope limiters even in the case of degenerate diffusion coefficients [25]. The space Q_h is equipped with the following semi-norm:

$$|q_h|_{Q_h} = \Big(\sum_{E\in\mathcal{E}^h} \|\nabla q_h\|^2_{L^2(E)} + \sum_{e\in\Gamma^h} |e|^{-1}\|\sigma^{1/2}[q_h]\|^2_{L^2(e)}\Big).$$

We now recall the coercivity property of the form a_T: there is a constant $\kappa > 0$ such that

$$\forall q_h \in Q_h, \quad a_T(\boldsymbol{U}^h; q_h, q_h) \geq \kappa |q_h|^2_{Q_h} + \|(\mathcal{U}^+)^{1/2} q_h\|^2_{L^2(\partial\Omega)}. \tag{34}$$

This is straightforward for the NIPG method ($\epsilon = 1$) and in that case the constant $\kappa = \min(1, \alpha)$ where α is the lower bound for $\boldsymbol{F}(\boldsymbol{u})$. For the SIPG method ($\epsilon = -1$), we use the fact that the matrix $\boldsymbol{F}(\boldsymbol{U}^h)$ is bounded above and the coercivity is obtained if the penalty parameter is large enough.

We will use the following inverse inequality. There is a constant $M > 0$ independent of h such that

$$\forall q_h \in Q_h, \forall E \in \mathcal{E}^h, \quad \|q_h\|_{L^\infty(E)} \leq M h^{-1} \|q_h\|_{L^2(E)}. \tag{35}$$

3.2.1 Existence and uniqueness of concentration

As the system is linear, it suffices to show uniqueness. Clearly the initial concentration is uniquely defined. Fix $j \geq 0$. Let $\theta_h = C_h^{j+1} - \tilde{C}_h^{j+1}$ be the difference of two solutions of (33). The function θ_h satisfies

$$\frac{\varphi}{\Delta t}\|\theta_h\|^2_{L^2(\Omega)} + a_T(\boldsymbol{U}^h; \theta_h, \theta_h) + d_T(\boldsymbol{U}^h; \theta_h, \theta_h) = 0.$$

Next, we use the coercivity (34) of a_T:

$$\frac{\varphi}{\Delta t}\|\theta_h\|^2_{L^2(\Omega)} + \kappa|\theta_h|^2_{Q_h} \leq |d_T(\boldsymbol{U}^h; \theta_h, \theta_h)|.$$

The first term in $d_T(\boldsymbol{U}^h; \theta_h, \theta_h)$ is bounded using Cauchy-Schwarz's inequality, Young's inequality, the inverse inequality (35) and the bound (32).

$$\begin{aligned}
|\sum_{E\in\mathcal{E}^h} (\theta_h \boldsymbol{U}^h, \nabla\theta_h)_E| &\leq \sum_{E\in\mathcal{E}^h} \|\theta_h\|_{L^\infty(E)} \|\boldsymbol{U}^h\|_{L^2(E)} \|\nabla\theta_h\|_{L^2(E)} \leq M h^{-1} \sum_{E\in\mathcal{E}^h} \|\theta_h\|_{L^2(E)} \|\boldsymbol{U}^h\|_{L^2(E)} \|\nabla\theta_h\|_{L^2(E)} \\
&\leq M\overline{M} h^{-1} \sum_{E\in\mathcal{E}^h} \|\theta_h\|_{L^2(E)} \|\nabla\theta_h\|_{L^2(E)} \leq \frac{M^2\overline{M}^2}{\kappa h^2}\|\theta_h\|^2_{L^2(\Omega)} + \frac{\kappa}{4}\sum_{E\in\mathcal{E}^h}\|\nabla\theta_h\|^2_{L^2(E)}.
\end{aligned}$$

The second term in $d_T(\boldsymbol{U}^h; \theta_h, \theta_h)$ is bounded similarly, but here we take advantage of the penalty term:

$$\begin{aligned}
|\sum_{e\in\Gamma^h} (\theta_h^\uparrow \{\boldsymbol{U}^h \cdot \boldsymbol{n}_e\}, [\theta_h])_e| &\leq M \sum_{e\in\Gamma^h} |e|^{-1/2} \|\sigma^{1/2}[\theta_h]\|_{L^2(e)} h^{1/2} \|\theta_h^\uparrow\|_{L^\infty(e)} \|\{\boldsymbol{U}^h \cdot \boldsymbol{n}_e\}\|_{L^2(e)} \\
&\leq M \sum_{e\in\Gamma^h} |e|^{-1/2} \|\sigma^{1/2}[\theta_h]\|_{L^2(e)} h^{1/2} h^{-1} \|\theta_h\|_{L^2(E_e^{12})} \|\{\boldsymbol{U}^h \cdot \boldsymbol{n}_e\}\|_{L^2(e)} \\
&\leq M \sum_{e\in\Gamma^h} |e|^{-1/2} \|\sigma^{1/2}[\theta_h]\|_{L^2(e)} h^{1/2} h^{-1} \|\theta_h\|_{L^2(E_e^{12})} h^{-1/2} \|\boldsymbol{U}^h\|_{L^2(E_e^{12})}.
\end{aligned}$$

In the bound above we have used the inverse inequality $\|\boldsymbol{U}^h\|_{L^2(e)} \leq M h^{-1/2} \|\boldsymbol{U}^h\|_{L^2(E)}$. We also defined the union of the elements who share the edge e by E_e^{12}. Next, we use the bound on the discrete velocity (32) and we obtain by Young's inequality:

$$|\sum_{e\in\Gamma^h} (\theta_h^\uparrow \{\boldsymbol{U}^h \cdot \boldsymbol{n}_e\}, [\theta_h])_e| \leq \frac{M^2\overline{M}^2}{h^2\kappa}\|\theta_h\|^2_{L^2(\Omega)} + \frac{\kappa}{4}\sum_{e\in\Gamma^h} |e|^{-1}\|\sigma^{1/2}[\theta_h]\|^2_{L^2(e)}.$$

Therefore we have

$$(\frac{\varphi}{\Delta t} - \frac{2M^2\overline{M}^2}{\kappa h^2})\|\theta_h\|^2_{L^2(\Omega)} + \frac{3\kappa}{4}|\theta_h|^2_{Q_h} \leq 0.$$

We conclude that $\theta_h = 0$ if the time step satisfies the following condition:

$$\Delta t < \frac{\kappa h^2 \varphi}{2M^2\overline{M}^2}.$$

We summarize our result below.

Lemma 3.1. *There is a constant $M_0 > 0$ such that if $\Delta t < M_0 h^2$, there is a unique solution to the scheme (33).*

3.2.2 Error analysis

We decompose the error at each time step into an approximation error η and a numerical error ξ. Let $\tilde{c} \in Q_h \cap \mathcal{C}(\overline{\Omega})$ be an approximation of c in the sense that the following approximation bounds [6] hold:

$$\|c(t^j) - \tilde{c}(t^j)\|_{L^2(\Omega)} \leq Mh^{r+1}\|c(t^j)\|_{H^{r+1}(\Omega)}, \quad \|\nabla(c(t^j) - \tilde{c}(t^j))\|_{L^2(\Omega)} \leq Mh^r\|c(t^j)\|_{H^{r+1}(\Omega)},$$

$$\|c(t^j) - \tilde{c}(t^j)\|_{L^\infty(\Omega)} \leq Mh^{r+1}\|c(t^j)\|_{H^{r+1}(\Omega)}, \quad \|\nabla(c(t^j) - \tilde{c}(t^j))\|_{L^\infty(\Omega)} \leq Mh^r\|c(t^j)\|_{H^{r+1}(\Omega)}.$$

We write

$$C_h^j - c(t^j) = \eta^j - \xi^j, \quad \eta^j = C_h^j - \tilde{c}(t^j), \quad \xi^j = c(t^j) - \tilde{c}(t^j).$$

Theorem 3.2. *Under the assumption of Lemma 3.1 and the additional regularity assumptions $c \in L^2(0,T;H^{r+1}(\Omega)) \cap W^{1,\infty}(\Omega)$, $c_t \in L^2(0,T;H^r(\Omega))$, and $c_0 \in H^r(\Omega)$, there is a constant M independent of h and Δt such that for all $m \geq 1$, and for Δt small enough, we have the error bound*

$$\|\eta^m\|^2_{L^2(\Omega)} + \kappa\Delta t\sum_{j=1}^m |\eta^j|^2_{Q_h} + \Delta t\sum_{j=1}^m \||\mathcal{U}|^{1/2}\eta^j\|^2_{\partial\Omega} \leq M(h^{2r} + h^{2k_1} + h^{2k_2} + \Delta t^2).$$

Proof. The error equation becomes

$$\begin{aligned}\forall q_h \in Q_h, \quad (\varphi\frac{\eta^{j+1} - \eta^j}{\Delta t}, q_h)_\Omega + a_T(\boldsymbol{U}^h; \eta^{j+1}, q_h) + d_T(\boldsymbol{u}; \eta^{j+1}, q_h) = (\varphi\frac{\partial\xi}{\partial t}(t^{j+1}), q_h)_\Omega + (\varphi\frac{\partial\tilde{c}}{\partial t}(t^{j+1}) - \varphi\frac{\tilde{c}^{j+1} - \tilde{c}^j}{\Delta t}, q_h)_\Omega \\ + d_T(\boldsymbol{u} - \boldsymbol{U}^h; \eta^{j+1}, q_h) + a_T(\boldsymbol{U}^h; \xi^{j+1}, q_h) + d_T(\boldsymbol{U}^h; \xi^{j+1}, q_h) + d_T(\boldsymbol{u} - \boldsymbol{U}^h; c(t^{j+1}), q_h) \\ + a_T(\boldsymbol{u}; c(t^{j+1}), q_h) - a_T(\boldsymbol{U}^h; c(t^{j+1}), q_h).\end{aligned}$$

We take $q_h = \eta^{j+1}$ and we use the coercivity (34) of a_T:

$$\begin{aligned}\frac{\varphi}{2\Delta t}(\|\eta^{j+1}\|^2_{L^2(\Omega)} - \|\eta^j\|^2_{L^2(\Omega)}) + \kappa|\eta^{j+1}|^2_{Q_h} + d_T(\boldsymbol{u}; \eta^{j+1}, \eta^{j+1}) + \|(\mathcal{U}^+)^{1/2}\eta^{j+1}\|^2_{L^2(\partial\Omega)} \leq |(\frac{\partial\xi}{\partial t}(t^{j+1}), \eta^{j+1})_\Omega| \\ + |(\frac{\partial\tilde{c}}{\partial t}(t^{j+1}) - \frac{\tilde{c}^{j+1} - \tilde{c}^j}{\Delta t}, \eta^{j+1})_\Omega| + |d_T(\boldsymbol{u} - \boldsymbol{U}^h; \eta^{j+1}, \eta^{j+1})| + |a_T(\boldsymbol{U}^h; \xi^{j+1}, \eta^{j+1})| \\ + |d_T(\boldsymbol{U}^h; \xi^{j+1}, \eta^{j+1})| + |d_T(\boldsymbol{u} - \boldsymbol{U}^h; c(t^{j+1}), \eta^{j+1})| + |a_T(\boldsymbol{u}; c(t^{j+1}), \eta^{j+1}) - a_T(\boldsymbol{U}^h; c(t^{j+1}), \eta^{j+1})|. \quad (36)\end{aligned}$$

Since the weak solution satisfies $\nabla \cdot \boldsymbol{u}|_{\Omega_1} = \boldsymbol{0}$ and $\nabla \cdot \boldsymbol{u}|_{\Omega_2} = f_2 \geq 0$, we use integration by parts and obtain:

$$d_T(\boldsymbol{u}; \eta^{j+1}, \eta^{j+1}) + \|(\mathcal{U}^+)^{1/2}\eta^{j+1}\|^2_{L^2(\partial\Omega)} = \frac{1}{2}(\mathcal{U}^+, (\eta^{j+1})^2)_{\partial\Omega} + \frac{1}{2}(\mathcal{U}^-, (\eta^{j+1})^2)_{\partial\Omega} \geq 0.$$

We now bound the first and second terms in the right-hand side of (36), by the approximation properties, under the regularity assumption for the exact solution c.

$$|(\frac{\partial\xi}{\partial t}(t^{j+1}), \eta^{j+1})_\Omega| \leq \|\eta^{j+1}\|^2_{L^2(\Omega)} + Mh^{2r}\|\frac{\partial c}{\partial t}(t^{j+1})\|^2_{H^r(\Omega)},$$

and

$$|(\frac{\partial \tilde{c}}{\partial t}(t^{j+1}) - \frac{\tilde{c}^{j+1} - \tilde{c}^j}{\Delta t}, \eta^{j+1})_\Omega| \leq \|\eta^{j+1}\|^2_{L^2(\Omega)} + \frac{\Delta t}{12}\int_{t^j}^{t^{j+1}} \|\frac{\partial^2 \tilde{c}}{\partial t^2}\|^2_{L^2(\Omega)}.$$

We now bound the d_T terms. Using standard techniques and inequality (35), we obtain

$$d_T(\boldsymbol{u} - \boldsymbol{U}^h; \eta^{j+1}, \eta^{j+1}) \leq M h^{-1} \|\eta^{j+1}\|_{L^2(\Omega)} \|\boldsymbol{u} - \boldsymbol{U}^h\|_{L^2(\Omega)} |\eta^{j+1}|_{Q_h}.$$

Using the velocity bound (30) and the fact that $k_1 \geq 1, k_2 \geq 1$, we have

$$d_T(\boldsymbol{u} - \boldsymbol{U}^h; \eta^{j+1}, \eta^{j+1}) \leq \frac{\kappa}{8}|\eta^{j+1}|^2_{Q_h} + M\|\eta^{j+1}\|^2_{L^2(\Omega)}.$$

Similarly, using (32), we have

$$d_T(\boldsymbol{U}^h; \xi^{j+1}, \eta^{j+1}) \leq M\|\xi^{j+1}\|_{L^\infty(\Omega)} \|\boldsymbol{U}^h\|_{L^2(\Omega)} |\eta^{j+1}|_{Q_h} \leq M\|\xi^{j+1}\|_{L^\infty(\Omega)} |\eta^{j+1}|_{Q_h}.$$

and using (30), (31) and the boundedness of the weak solution, we have

$$\begin{aligned} d_T(\boldsymbol{u} - \boldsymbol{U}^h; c(t^{j+1}), \eta^{j+1}) &\leq M\|c(t^{j+1})\|_{L^\infty(\Omega)} |\eta^{j+1}|_{Q_h} \big(\|\boldsymbol{u} - \boldsymbol{U}^h\|_{L^2(\Omega)} + (\sum_{e\in\Gamma^h} |e| \|\boldsymbol{u} - \boldsymbol{U}^h\|^2_{L^2(e)})^{1/2}\big) \\ &\leq \frac{\kappa}{8}|\eta^{j+1}|^2_{Q_h} + M(h^{2k_1} + h^{2k_2}). \end{aligned}$$

The diffusive term $a_T(\boldsymbol{U}^h; \xi^{j+1}, \eta^{j+1})$ is bounded using standard techniques.

$$a_T(\boldsymbol{U}^h; \xi^{j+1}, \eta^{j+1}) \leq \frac{\kappa}{8}|\eta^{j+1}|^2_{Q_h} + \frac{1}{8}\|(\mathcal{U}^+)^{1/2}\eta^{j+1}\|^2_{L^2(\partial\Omega)} + Mh^{2r}\|c(t^{j+1})\|^2_{H^{r+1}(\Omega)}.$$

To bound the remaining diffusive terms, we use the boundedness of c, the Lipschitz continuity of F and the bounds (30), (31).

$$a_T(\boldsymbol{u}; c(t^{j+1}), \eta^{j+1}) - a_T(\boldsymbol{U}^h; c(t^{j+1}), \eta^{j+1}) \leq \frac{\kappa}{8}|\eta^{j+1}|^2_{Q_h} + M(h^{2k_1} + h^{2k_2}).$$

We can now conclude by combining all bounds, summing over the time steps, and using Gronwall's inequality. □

4 Numerical examples

In this section, we show that our schemes are robust under different physical conditions (faults, discontinuous permeability field). We also investigate the effect of different approximations of velocity on the concentration solution. In all the numerical examples, the fluid viscosity is equal to 1, and the Beavers-Joseph-Saffman constant to 0.1. Meshes are generated using Gmsh [17], visualization is done using Tecplot [1] and the simulations are done using software developed by the authors. Uniqueness of the pressure is obtained by imposing a Dirichlet boundary condition on part of the subsurface boundary.

4.1 Step interface

In the first example, the rectangular domain $\Omega = (0, 2) \times (0, 1.25)$ is partitioned into two subdomains by a polygonal interface with three successive uniform steps (see Fig. 1). For the flow problem, the Stokes equations are solved in Ω_1 and the Darcy equations in Ω_2. The permeability of Ω_2 is $\boldsymbol{K} = 10^{-4}\boldsymbol{I}$. Zero Dirichlet boundary conditions are imposed on the bottom horizontal side of Ω_2 and zero Neumann boundary conditions on the remainder of $\Omega_2 \setminus \Gamma_{12}$. The Stokes velocity on Γ_1 is set equal to $(-3(y - 1.25)(y - 0.5), 0)$, which means the velocity profile is parabolic along the vertical side of Γ_1. The pressure contours and Euclidean norm of velocity contours with streamlines are shown in Fig. 2. The DG scheme is used with $\epsilon = 1$, $\sigma = 0.1$

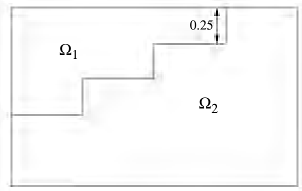

Figure 1: Domain with step interface.

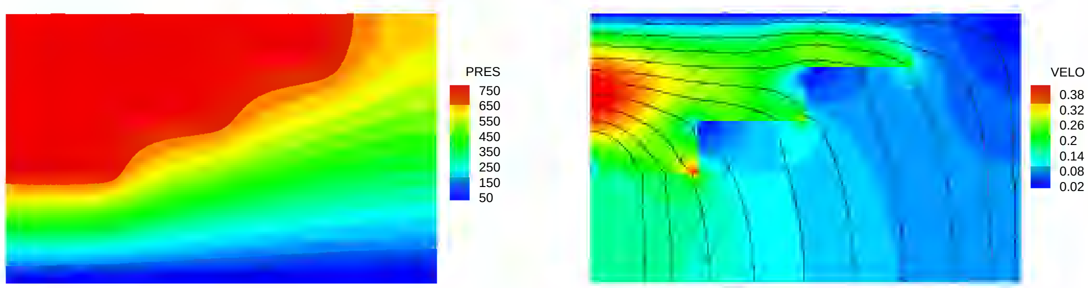

Figure 2: Step interface problem: pressure contours (left) and velocity norm and streamlines (right).

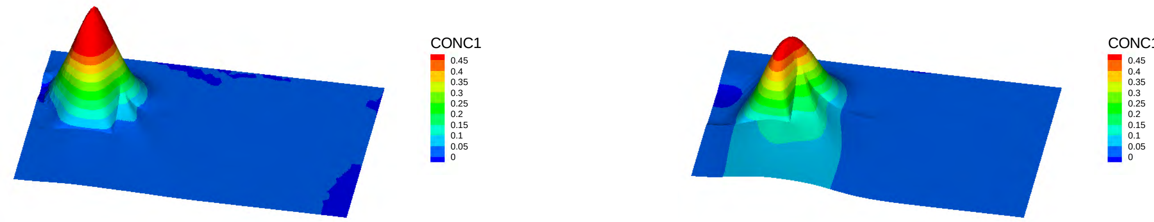

Figure 3: Concentration contours at $t = 1$ (left) and $t = 1.5$ (right).

and $k_1 = k_2 = 2$. The mesh contains 5760 triangles of varying size so that the triangles in the neighborhood of the interface are the smallest. We now describe the characteristics of the transport problem for this example. The coefficients are: $\varphi = 0.2$, $\alpha_l = 1$, $\alpha_t = 0.1$, $c_0 = \mathcal{C} = 0$, $d_m = 10^{-3}$ in Ω_2, $d_m = 5 \times 10^{-3}$ in Ω_1. In this example, we simulate the leakage of a contaminant in the surface by the source function:

$$f(t,x,y) = \begin{cases} 1, & t < 1, \text{ and } ((x-0.2)^2 + (y-0.85)^2)^{1/2} \leq 0.15 \\ 0, & \text{otherwise} \end{cases}$$

Concentration contours at the time $t = 1$ where the plume reaches its maximum peak are shown in Fig. 3 (left). At this time, the contaminant has just reached the interface. Concentration contours at later times are shown on Fig. 3 (right) and Fig. 4. Once the contaminant penetrates the subsurface it is transported downwards and exits the domain via the bottom horizontal boundary. The numerical approximation of the concentration is obtained with the DG method with $\epsilon = 1, r = 1, \sigma = 0.1$ and $\Delta t = 2.5 \times 10^{-3}$.

4.2 Non-uniform permeability field

In this second example, the permeability of the subsurface takes random values between $10^{-7}\boldsymbol{I}$ and $3.8 \times 10^{-5}\boldsymbol{I}$. The domain is $\Omega = (0,12) \times (0,6)$ and the interface is a horizontal line containing two steps of opposite direction. Fig 5 shows the domain and the permeability distribution.

First for the flow problem, we impose a parabolic velocity profile on the left vertical boundary of Ω_1 and a similar profile on the right vertical boundary of Ω_1 but with a smaller magnitude. Zero Neumann boundary conditions are imposed on the Darcy pressure for the vertical boundaries of Ω_2 and Dirichlet pressure is prescribed on bottom horizontal boundary. The Dirichlet values are given below:

$$\forall y \geq 4, \quad \boldsymbol{u}_1(0,y) = (0.25(y-4)(8-y), 0), \quad \boldsymbol{u}_1(12,y) = ((3/16)(y-4)(8-y), 0),$$
$$\forall 0 \leq x \leq 12, \quad \boldsymbol{u}_1(x,6) = (1,0), \quad p_2(x,0) = 10^5.$$

The Navier-Stokes equations are solved in Ω_1 and the Darcy equations in Ω_2. The mesh contains 562 triangles in the surface and 625 triangles in the subsurface. The DG method with parameters $\sigma = 1, \epsilon = 1, k_1 = k_2 = 2$ is used. The Picard iterations for the flow problem converge after 9 iterations, with a set tolerance of 10^{-7}.

Figure 4: Concentration contours at $t = 2.5$ (left) and $t = 4$ (right).

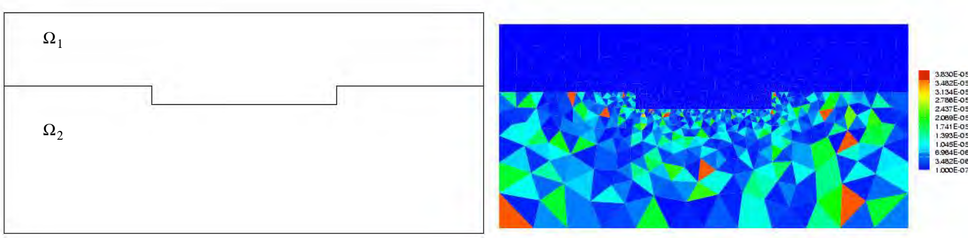

(a) (b)

Figure 5: Domain (a) and permeability field (b).

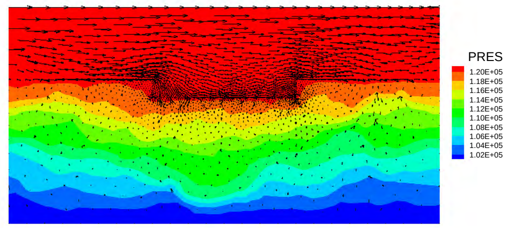

Figure 6: Pressure contours and velocity field.

Fig. 6 shows the pressure contours and the velocity field. Since the exact solution is unknown, we compute the differences between the solutions obtained on two successive meshes (i.e. of size h and $h/2$). We obtain a rate of $\mathcal{O}(h^{0.4})$ for the H^1 norm of the Navier-Stokes velocity and $\mathcal{O}(h^{0.4})$ for the H^1 norm of the Darcy pressure. These rates confirm convergence of the scheme for solutions with low regularity.

Second for the transport problem, the concentration is prescribed on the inflow boundary ($\mathcal{C} = 1$). The initial concentration is zero. The other parameters defining the problem are: $r = 1$, $\varphi = 0.2$, $\alpha_l = 0.1$, $\alpha_t = 0.01$, $d_m = 10^{-4}$ in Ω_2, $d_m = 10^{-2}$ in Ω_1. Discontinuous piecewise linear approximation of the concentration are obtained. Fig. 7, 8, 9 present the concentration contours at successive times. We observe that the contaminant sweeps the surface region very fast, then percolates down the subsurface at a slower rate. This is expected as the velocity in the subsurface is much smaller than the velocity in the surface. We also note that the contaminant is transported downwards in the subsurface in a non-uniform way. This is explained by the discontinuous distribution of the permeability field.

4.3 Fractured subsurface

In this last example, the porous medium $\Omega = (0, 12) \times (0, 6)$ contains three horizontal layers of varying permeability that are intersected by two slanted faults. The permeability matrix is equal to $10^{-4}\mathbf{I}$, $10^{-9}\mathbf{I}$, $10^{-5}\mathbf{I}$, $10^{-7}\mathbf{I}$ in the faults, the top layer, the middle layer and the bottom layer respectively (see Fig. 10). Boundary conditions for the flow problem are the same as in the previous example (Section 4.2). Fig. 11 shows the pressure contours and the velocity field obtained with the DG method of first and second order, which yields 8707 and 17679 degrees of freedom respectively. The pressure follows a vertical gradient, and thus the velocity in the middle layer (denoted by B on Fig. 10) remains small. For this example, we also solve the flow problem using the FEM/DG method of order one. The MINI elements are used for the Navier-Stokes region. Discontinuous piecewise linear or quadratic approximations are used in the Darcy region. Fig. 12 shows the pressure contours and streamlines obtained on the same mesh as the solutions in Fig. 11. Using FEM/DG is computationally cheaper than DG alone, as the number of degrees of freedom is 7899 and 14766 for piecewise linears and quadratics respectively. However we observe that even though the streamlines are similar, the values for the pressure differ. If we solve the problem on a finer mesh, the pressure values match those obtained by the DG scheme (see Fig. 13). The number of degrees of freedom is 125043 and 234915 for piecewise linears and quadratics respectively. Similar conclusions can be made if the FEM scheme is used in the whole domain. The method of order one yields the smallest number of degrees of freedom (2196), however the solution is not accurate enough and the mesh needs to be finer.

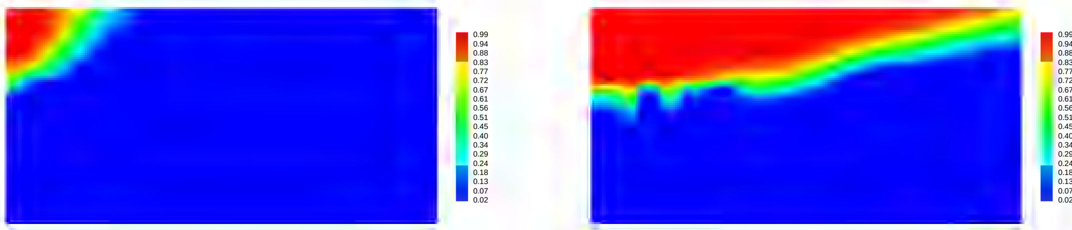

Figure 7: Concentration at different times: t_1 (left) and $t_2 = 6t_1$ (right).

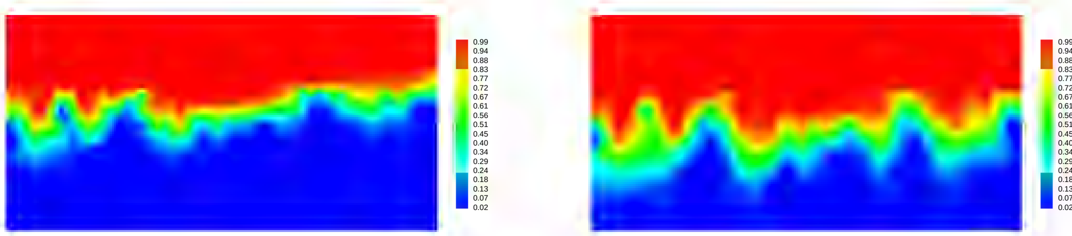

Figure 8: Concentration at different times: $t_3 = 16t_1$ (left) and $t_4 = 26t_1$ (right).

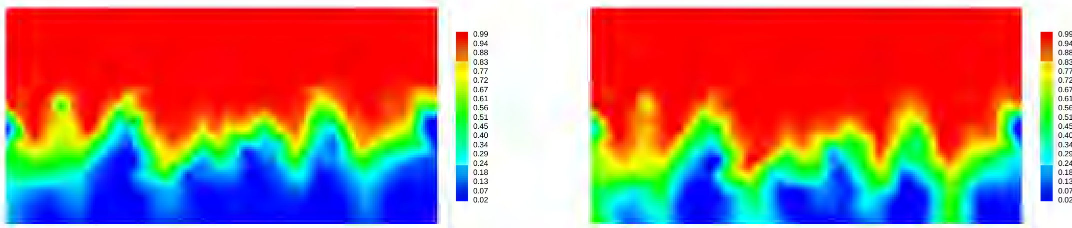

Figure 9: Concentration at different times: $t_5 = 32t_1$ (left) and $t_6 = 40t_1$ (right).

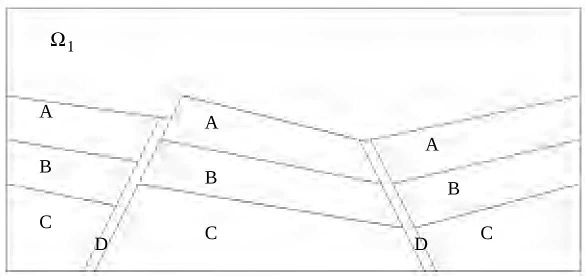

Figure 10: Domain for surface coupled with fractured subsurface. Permeability value is 10^{-9} in A region, 10^{-5} in B region, 10^{-7} in C region and 10^{-4} in D region (slanted fractures).

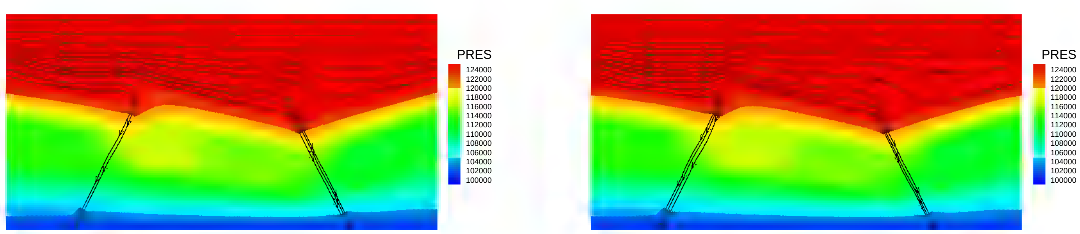

Figure 11: Pressure and velocity field obtained with the DG method of order one (left figure) and order two (right figure).

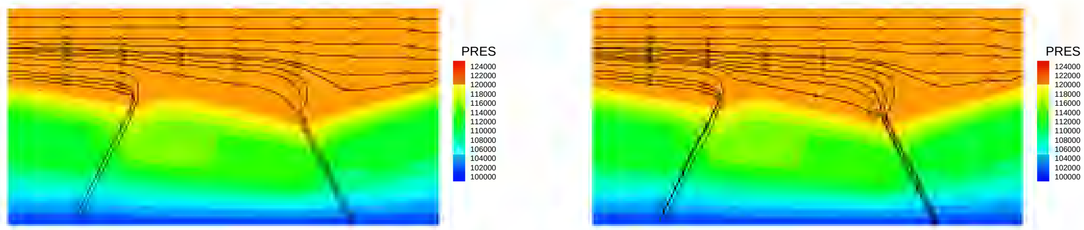

Figure 12: Pressure and velocity field obtained with the FEM/DG method of order one (left figure) and order two (right figure).

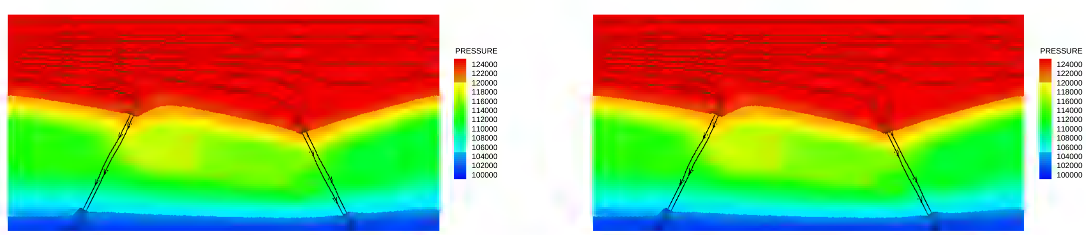

Figure 13: Pressure and velocity field obtained with the FEM/DG method of order one (left figure) and order two (right figure) on a very fine mesh.

Next we describe the parameters chosen for the transport problem. The coefficients are: $\varphi = 0.2$, $\alpha_l = 0.1$, $\alpha_t = 0.01$, $\mathcal{C} = 0$, $d_m = 10^{-4}$ in Ω_2, $d_m = 10^{-2}$ in Ω_1. As in the first example, we simulate the leakage of a contaminant in the surface. The initial concentration is equal to one in a localized region in the surface, and zero elsewhere. In addition, there is a temporary source of contaminant (for $t \leq t^*$, with $t^* = 3$) defined by:

$$f(t,x,y) = \begin{cases} 0.5, & t < 3, \text{ and } ((x-2.0)^2 + (y-5.1)^2)^{1/2} \leq 0.5 \\ 0, & \text{otherwise} \end{cases}$$

As in the previous two examples, we obtain the numerical approximation of the concentration by the DG method with parameters $r = \epsilon = \sigma = 1$. In Fig. 14, 15, 16, we show the concentration contours at different times in the case where the numerical approximation of the velocity is obtained by DG (with $k_1 = k_2 = 2$), FEM/DG (with $k_1 = 1$ and $k_2 = 2$) and FEM (with $k_1 = k_2 = 1$) schemes. We note that the mesh used for the transport problem is the same as the one used in Fig. 11 and Fig. 12. The overall behavior of the solution is as expected: the contaminant is transported faster in the surface region, and some of it penetrates the subsurface via the slanted fractures. Because of the intermediate value of the permeability in the middle layer, some of the contaminant appears in part of region B neighboring the fractures.

The interest of this example is to see that the poor/good accuracy of the input velocity has an important effect on the concentration solution. At the times t_1 and t_2, solutions obtained with FEM/DG or FEM input velocities are similar. At the time t_3 (which is greater than t^*, the time when the source disappears), we observe an unphysical accumulation of mass at the outflow boundary of the left fracture if the FEM velocity is used. The use of DG in the subsurface region for the flow problem removes this numerical problem. We also note that the solution obtained with DG input velocity differs from the other two solutions. The contaminant plume appears to be less diffusive, and further along the x-axis. This is particularly clear in Fig. 16, where we see that the left fracture contains very little contaminant if the input velocity is obtained with DG. In addition, a larger amount of contaminant has reached the second fracture.

5 Conclusions

The coupling of surface/subsurface flow and transport is studied theoretically and numerically by the use of finite element methods and discontinuous Galerkin methods. It is shown that the DG scheme is robust and yields accurate solutions for inhomogeneous or fractured subsurface. A finer mesh is needed to obtain an accurate FEM/DG or FEM velocity. If one is constrained to use the same computational mesh for both flow and transport, then the most economical solution is still given by the DG method. It would be of interest to study the effects of projection of the velocity field, if independent meshes are used for the flow and transport problems.

References

[1] http://www.tecplot.com/.

[2] H. W. Alt and S. Luckhaus. Quasilinear elliptic-parabolic differential equations. *Math. Z.*, 183(3):311–341, 1983.

[3] D.N. Arnold. An interior penalty finite element method with discontinuous elements. *SIAM J. Numer. Anal.*, 19:742–760, 1982.

[4] D.N Arnold, F.Brezzi, and M. Fortin. A stable finite element for the Stokes equations. *Calcolo*, 21(4):337–344, 1984.

[5] G.S. Beavers and D.D. Joseph. Boundary conditions at a naturally impermeable wall. *J. Fluid. Mech*, 30:197–207, 1967.

[6] S. C. Brenner and L. R. Scott. *The Mathematical Theory of Finite Element Methods*. Springer-Verlag, New York, 1994.

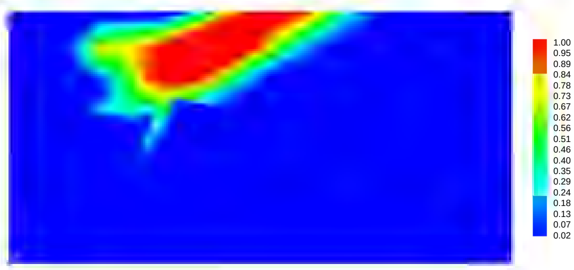

(a) Input DG

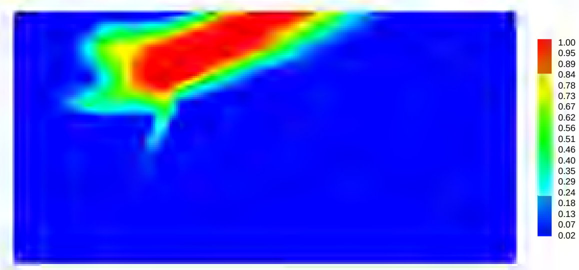

(b) Input FEM/DG

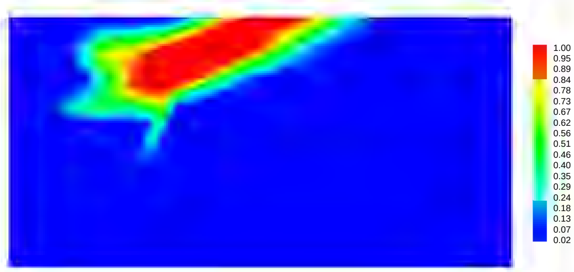

(c) Input FEM

Figure 14: Concentration contours at time t_1 with input velocity obtained from DG (a), FEM/DG (b) and FEM (c).

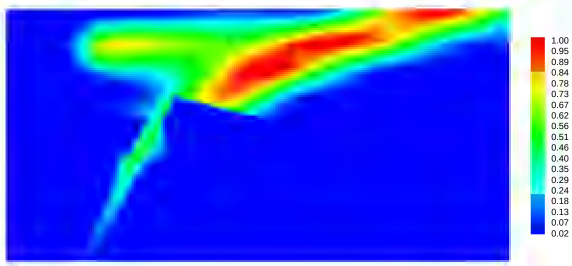

(a) Input DG

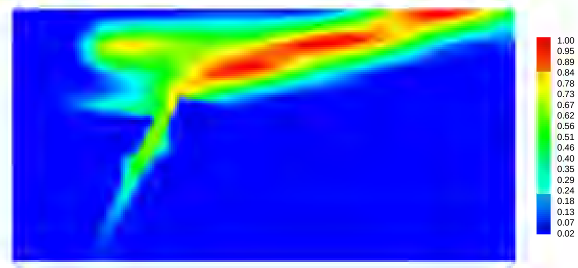

(b) Input FEM/DG

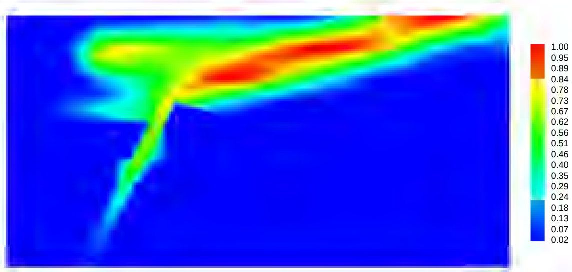

(c) Input FEM

Figure 15: Concentration contours at time $t_2 = 2t_1$ with input velocity obtained from DG (a), FEM/DG (b) and FEM (c).

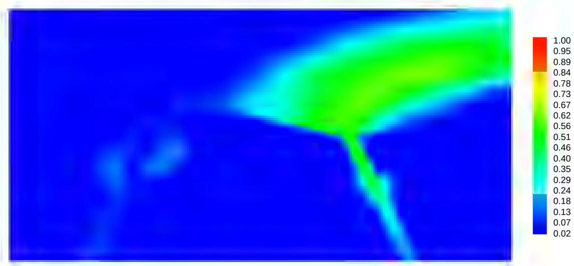

(a) Input DG

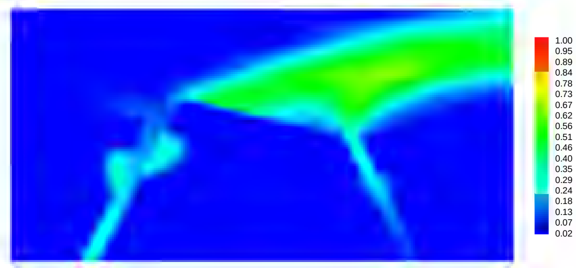

(b) Input FEM/DG

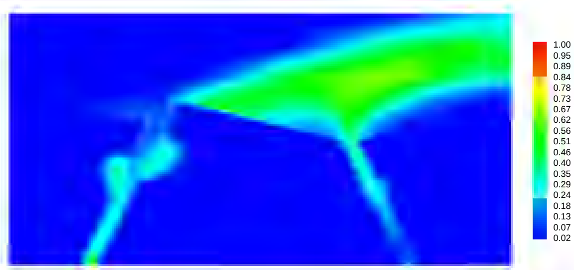

(c) Input FEM

Figure 16: Concentration contours at time $t_3 = 5t_1$ with input velocity obtained from DG (a), FEM/DG (b), and FEM (c).

[7] A. Cesmelioglu and B. Riviere. Analysis of weak solutions for the fully coupled Stokes-Darcy-Transport problem. technical report TR09-38, submitted to SIAM Journal on Mathematical Analysis.

[8] A. Cesmelioglu and B. Riviere. Analysis of time-dependent Navier-Stokes flow coupled with Darcy flow. *Journal of Numerical Mathematics*, 16:249–280, 2008.

[9] A. Cesmelioglu and B. Riviere. Primal discontinuous Galerkin methods for time-dependent coupled surface and subsurface flow. *Journal of Scientific Computing*, 40:115–140, 2009.

[10] P. Chidyagwai and B. Riviere. On the solution of the coupled Navier-Stokes and Darcy equations. *Computer Methods in Applied Mechanics and Engineering*, 198:3806–3820, 2009.

[11] P. Chidyagwai and B. Riviere. Numerical modelling of coupled surface and subsurface flow systems. *Advances in Water Resources*, 33:92–105, 2010.

[12] P. Ciarlet. *The finite element method for elliptic problems*. North-Holland, Amsterdam, 1978.

[13] B. Cockburn and C.-W. Shu. The local discontinuous Galerkin method for time-dependent convection-diffusion systems. *SIAM Journal on Numerical Analysis*, 35:2440–2463, 1998.

[14] M. Discacciati and A. Quarteroni. Analysis of a domain decomposition method for the coupling of Stokes and Darcy equations. In Brezzi et al, editor, *Numerical Analysis and Advanced Applications - ENUMATH 2001*, pages 3–20. Springer, Milan, 2003.

[15] M. Discacciati, A. Quarteroni, and A. Valli. Robin-Robin domain decomposition methods for the Stokes-Darcy coupling. *SIAM J. Numer. Anal.*, 45(3):1246–1268, 2007.

[16] G.N. Gatica, R. Oyarza, and F.-J. Sayas. Convergence of a family of Galerkin discretizations for the Stokes-Darcy coupled problem. *Numerical Methods for Partial Differential Equations*, 2009. DOI: 10.1002/num.20548.

[17] C. Geuzaine and J.-F. Remacle. Gmsh: a three-dimensional finite element mesh generator with built-in pre- and post-processing facilities. *International Journal for Numerical Methods in Engineering*, 79:1309–1331, 2009. http://www.geuz.org/gmsh/.

[18] V. Girault and B. Riviere. DG approximation of coupled Navier-Stokes and Darcy equations by Beaver-Joseph-Saffman interface condition. *SIAM Journal on Numerical Analysis*, 47:2052–2089, 2009.

[19] V. Girault, B. Rivière, and M. Wheeler. A discontinuous Galerkin method with non-overlapping domain decomposition for the Stokes and Navier-Stokes problems. *Mathematics of Computation*, 74:53–84, 2004.

[20] N.S. Hanspal, A.N. Waghode, V. Nassehi, and R.J. Wakeman. Numerical analysis of coupled Stokes/Darcy flows in industrial filtrations. *Transport in Porous Media*, 64(1):1573–1634, 2006.

[21] P. Hood and C. Taylor. A numerical solution of the Navier-Stokes equations using the finite element technique. *Comp. and Fluids*, 1:73–100, 1973.

[22] W.J. Layton, F. Schieweck, and I. Yotov. Coupling fluid flow with porous media flow. *SIAM J. Numer. Anal.*, 40(6):2195–2218, 2003.

[23] F. Marpeau and M. Saad. Mathematical analysis of radionuclides displacement in porous media with nonlinear adsorption. *J. Differ. Equations*, 228(2):412–439, 2006.

[24] M. Mu and J. Xu. A two-grid method of a mixed Stokes-Darcy model for coupling fluid flow with porous media flow. *SIAM Journal on Numerical Analysis*, 45:1801–1813, 2007.

[25] J. Proft and B. Riviere. Discontinuous Galerkin methods for convection-diffusion equations with varying and vanishing diffusivity. *International Journal of Numerical Analysis and Modeling*, 6:533–561, 2009.

[26] B. Rivière, M.F. Wheeler, and V. Girault. A priori error estimates for finite element methods based on discontinuous approximation spaces for elliptic problems. *SIAM Journal on Numerical Analysis*, 39(3):902–931, 2001.

[27] P. Saffman. On the boundary condition at the surface of a porous media. *Stud. Appl. Math.*, 50:292–315, 1971.

[28] D. Vassilev and I. Yotov. Coupling Stokes-Darcy flow with transport. *SIAM Journal on Scientific Computing*, 31(5):3661–3684, 2009.

[29] M.F. Wheeler. An elliptic collocation-finite element method with interior penalties. *SIAM Journal on Numerical Analysis*, 15(1):152–161, 1978.